Macromolecules

ARTICLE

pubs.acs.org/Macromolecules

Microstructure and Mechanical Properties of Polypropylene/Poly(methyl methacrylate) Nanocomposite Prepared Using Supercritical Carbon Dioxide

Rui Zhu,[*,†] Toru Hoshi,[‡,§] Yoshihiro Chishima,[‡] Yoshio Muroga,[‡,⊥] Toshiki Hagiwara,[‡] Shoichiro Yano,[‡,⊥] and Takashi Sawaguchi[*,‡,⊥]

[†]Department of Materials and Applied Chemistry, Graduate School of Science and Technology, Nihon University, 1-8-14, Kanda-surugadai, Chiyoda-ku, Tokyo 101-8308, Japan

[‡]Department of Materials and Applied Chemistry, College of Science and Technology, Nihon University, 1-8-14, Kanda-surugadai, Chiyoda-ku, Tokyo 101-8308, Japan

[§]Center for Creative Materials Research, Research Institute of Science and Technology, College of Science and Technology, Nihon University, 1-8-14, Kanda-surugadai, Chiyoda-ku, Tokyo 101-8308, Japan

[⊥]Research Institute of Science and Technology, College of Science and Technology, Nihon University, 1-8-14, Kanda-surugadai, Chiyoda-ku, Tokyo 101-8308, Japan

ABSTRACT: A novel composite comprising polypropylene (PP) and poly(methyl methacrylate) (PMMA) was prepared using supercritical carbon dioxide ($scCO_2$), although the two polymers are usually immiscible and have phase-separated morphology. This paper reports in detail the preparation, microstructure, crystallinity, and thermodynamic and mechanical properties of the PP/PMMA composite. The microstructure of the PP/PMMA composite was investigated using transmission electron microscopy (TEM), atomic force microscopy (AFM), and small-angle X-ray scattering (SAXS), and these measurements yielded consistent results. PP and PMMA were blended at the nanometer level through the supercritical impregnation of a methyl methacrylate (MMA) monomer and an initiator into the amorphous interlamellar regions of a PP substrate, followed by *in situ* polymerization of the MMA monomers. The PMMA produced within the PP is of high molecular weight. The results of wide-angle X-ray diffraction (WAXD) and differential scanning calorimetry (DSC) showed that PMMA did not affect the crystallinity, the enthalpy of melting the PP crystal, or the top temperature of the PP crystal melting, but it did reduce the starting temperature at which the PP crystal melting. The dynamic viscoelastic measurements and tensile tests were used to measure the mechanical properties of the composite including storage modulus, yield stress, fracture stress, and strain. It was determined that these properties depended on the composition of the composite and are dependent on the initial pressure of CO_2. The dynamic viscoelastic measurements also showed that the PP and PMMA were somewhat thermodynamically miscible.

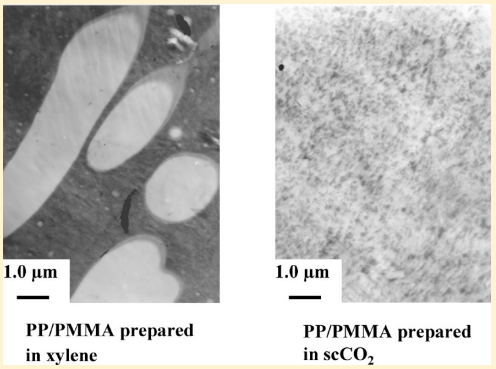

INTRODUCTION

The blending of two or more polymers with different characteristics is one of the most important techniques used to prepare new materials with novel features not found in any current constituent polymer. In general, the miscibility of different polymers is so limited that conventional methods such as melt processing or casting from solution have only been successfully employed in a few cases, e.g., the polystyrene (PS)/poly(vinyl methyl ether) blend.[1] Amorphous polymers and semicrystalline polymers cannot be blended using conventional methods because the amorphous polymer is excluded from the crystalline regions during the crystal growth process.[2]

A synthetic method for producing new polymer composites using supercritical carbon dioxide ($scCO_2$) has been developed by Watkins and McCarthy.[3] Both the monomer and initiator are dissolved in $scCO_2$ and then impregnated into the polymer substrate and subsequently polymerized. Using this method, we have already succeeded in obtaining microphase-separated polymer composites of polyethylene (PE)/poly(vinyl acetate) (PVAc) and syndiotactic polystyrene (sPS)/poly(methyl methacrylate) (PMMA), even though they are immiscible and thus could not have been obtained using conventional methods.[4,5] The PE/PVAc composite features a biocompatible surface and could be used to fabricate medical devices. The sPS/PMMA composite was blended at the nanometer level, and thus, favorable mechanical properties are expected. PS composites of semicrystalline and glassy polymer substrates such as polyethylene (PE), bisphenol A polycarbonate, poly(oxymethylene), nylon-66,

Received: February 3, 2011
Revised: July 7, 2011
Published: July 18, 2011

poly(4-methyl-l-pentene), and poly(chlorotrifluoroethylene) were also successfully synthesized.[3,6,7] Kung et al. reported that mechanical properties such as Young's modulus and the yield stress of high-density polyethylene (HDPE)/PS composites obtained using $scCO_2$ could be controlled by composition.[8] In addition, they showed that the mechanical properties of the HDPE/PS composite prepared using $scCO_2$ were superior to a HDPE/PS blend prepared using the conventional melt-mixing process. Ultrahigh-molecular-weight polyethylene (UHMWPE)/methacrylate polymer composites prepared with various hydrophobic methacrylate monomers featuring alkyl side chains of varying lengths in place of the styrene and the controlled preparation of copolymer blends of alky methacrylates within a UHMWPE substrate have also been reported.[9−11] UHMWPE was also blended with biodegradable polymers—polycaprolactone (PCL)—successfully.[12] Moreover, semi-interpenetrating polymer networks (IPNs) of UHMWPE with PMMA-*co*-poly(ethylene glycol) dimethacrylate (PEGDMA) were prepared through $scCO_2$ facilitated impregnation of MMA and ethylene glycol dimethacrylate (EGDMA) monomers into UHMWPE.[13] The mechanical properties of polymer composites prepared using the $scCO_2$ method can be controlled by using a combination of the substrate and monomer.

Polypropylene (PP) is one of the largest volume polyolefins in the plastics industry. It has many desirable physical properties including low density, high melting temperature, high tensile modulus, and excellent chemical resistance.[14] Combined with its low cost, these properties make PP ideal for a variety of applications including appliances, packaging, textiles, reinforcing fibers, monofilaments, films, automotive parts, reusable containers of various types, and other durable items for home and garden use. Additionally, the ranges of applications for PP can also be extended by various physical treatments, for example, thermal treatment[15−17] and plastic deformation.[18,19]

However, PP has the disadvantages such as low surface energy, lack of chemical functionalities, difficulty to dye. Moreover, when a polymer composite of PP and other polymers is prepared, phase separation occurs, and a macrodomain structure is formed because of the crystal growth of PP from the melt or soluble state.[2] The properties of PP such as storage modulus, yield stress, fracture stress, and strain could be changed through the blending of another amorphous polymer into the amorphous phases of PP to meet various needs. PMMA is an amorphous polymer having high optical properties, good chemical resistance, and high tensile strength. The present study establishes a method to prepare a new nanocomposite material with PMMA dispersed on a nanometer scale in the amorphous phase of PP. PP and PMMA have quite different physical properties and cannot be sufficiently blended using conventional methods. In this study, $scCO_2$ is used as a processing medium to facilitate effective impregnation of methyl methacrylate (MMA) monomer into the amorphous phase of PP, followed by radical-initiated *in situ* polymerization.

To date, although there is extensive work in the area of semicrystallilne/amorphous polymer composites (such as PE/amorphous polymer composites) prepared in $scCO_2$, the study of PP as a polymer substrate is few. Additionally, changes of melting temperature of substrate polymer after blending with an amorphous polymer, thermodynamic miscibility of respective component, and thermal stability of the composites (this will be discussed in our next paper) have not been evaluated. In this paper, the details of the preparation of a PP/PMMA composite are first reported. We investigate the microstructure of the composite by combining transmission electron microscopy (TEM), atomic force microscopy (AFM), and small-angle X-ray scattering (SAXS). The crystallinity of the composite was investigated by wide-angle X-ray diffraction (WAXD), and the melting temperature and enthalpy of crystal were determined by differential scanning calorimetry (DSC). The mechanical properties of the composite were analyzed by means of dynamic viscoelastic measurements and tensile tests. The thermodynamic miscibility was evaluated by DSC and dynamic viscoelastic measurements.

EXPERIMENTAL SECTION

Materials. An isotactic polypropylene substrate was prepared from a commercially obtained pellet (Mitsui Chemical, Inc., Tokyo, Japan) by hot pressing at 190 °C. The substrate was cut into pieces with dimensions of 20 × 20 × 0.5 mm^3, extracted with acetone for 24 h in a Soxhlet extractor, and dried *in vacuo* at room temperature. MMA and acetone were purchased, and used without further purification, from Wako Pure Chemical Industries, Ltd., Tokyo, Japan, and Kanto Chemical Co., Tokyo, Japan, respectively. 2,2′-Azobis(isobutyronitrile) (AIBN) was purchased from Kanto Chemical Co., Inc., Japan, and used after recrystallization from methanol. Carbon dioxide, with a purity of 99.5%, was provided by Tomoe Shokai Co., Tokyo, Japan, and used as received.

Preparation of PP/PMMA Composite Using $scCO_2$. The sample was prepared in an apparatus consisting of a 50 mL stainless steel vessel, magnetic stirrer, constant-temperature air bath (Model SCF-Sro, JASCO Co., Tokyo, Japan), thermocouple, and pressure gauge. The pressure gauge comprised a transducer (Model PTX1400, Druck Japan Co., Tokyo, Japan) and an indicator, which had a precision of ±0.2% in the pressure range of 0−40 MPa. The PP substrate was suspended in the vessel by means of a wire mesh to ensure that no part of the substrate was in contact with the monomer solution or the vessel wall. The PP substrate, MMA monomer (2 g), and AIBN initiator (0.03 g) were placed in the vessel, which was then sealed.[9] The vessel was then flushed by CO_2 at atmospheric pressure. After the system reached thermal equilibrium (35 °C), the vessel was pressurized up to a specific CO_2 pressure using a CO_2 delivery pump (Model SCF-Get, JASCO Co., Tokyo, Japan). The PP substrate was soaked for 1 h. The vessel was then pressurized to the last specific pressure (to compensate for the drop in pressure due to dissolution of the monomer and initiator), heated to the reaction temperature (80 °C), and held for 24 h to ensure that the polymerization of MMA was complete. The vessel was then cooled to 10 °C and gradually returned to ambient pressure. After extracting the sample with acetone for 24 h to remove unreacted reagents and the surface PMMA using a Soxhlet extractor, the PP/PMMA composite was dried *in vacuo* at room temperature. The mass gain was calculated using the following equation:

$$\text{mass gain (wt \%)} = \frac{W_t - W_0}{W_0} \times 100 \quad (1)$$

where W_0 is the initial weight of PP substrate and W_t is the weight of PP/PMMA composite sheet after drying. The density of the sample was calculated using the following equation:

$$\textit{density}\ (g/cm^3) = \frac{W_t}{L^2 \times T} \quad (2)$$

where L is the average length of the four sides and T is the thickness of the PP/PMMA composite sample. The length and thickness were measured at room temperature. The molecular weight of PMMA produced inside and outside PP substrate was determined by a gel permeation chromatograph (GPC) with THF as the mobile phase.

The PMMA produced inside of PP substrate was separated using the following method: The PP/PMMA composite was dissolved in hot xylene. This solution was precipitated into acetone. The precipitate (PP) was removed by filtration, and the remaining solution was rotary evaporated to isolate the PMMA.

A reference sample was also prepared for SAXS and other analyses from the solution as follows: equal masses of PP and PMMA were dissolved in xylene at reflux temperature, and the solution was poured into methanol to obtain the precipitate, which was vacuum-dried under heat. The obtained precipitate was shaped into a sheet following the same process as was used for the PP substrate.

Microstructure Analyses. TEM micrographs were recorded using a JEOL JEM-100CX transmission electron microscope at an accelerating voltage of 100 kV. RuO_4 was used to stain the composite specimens, which were cut into ultrathin sections at room temperature using an ultramicrotome.

AFM experiments were performed using a Nanoscope IIIa-controlled Dimension 3000 AFM (Digital Instruments, Santa Barbara, CA). Commercial silicon cantilever probes, with a nominal tip radius of less than 10 nm (Nanoscope Olympus, 160 μm cantilever length and spring constant ranging 12−103 N m^{-1}), were employed just under their fundamental resonance frequencies of about 300 kHz. Height and phase images were acquired simultaneously under ambient conditions. Scan rates were set at 2 Hz for all images.

SAXS experiments were carried out using synchrotron radiation as the X-ray source at the Photon Factory of the High Energy Accelerator Organization at Tsukuba, Ibaragi, Japan. The wavelength of the X-rays was 0.1488 nm, and the scattered intensity was detected using a one-dimensional position-sensitive proportional counter (PSPC) with 512 channels that was located about 2 m from the sample. The setup was calibrated on a sample of expanded chicken collagen, which gave a set of sharp diffractions corresponding to a Bragg spacing of 653 Å. The details of the instrumentation and procedure are described elsewhere.[20]

Crystallinity Analysis. WAXD experiments were performed at 20 °C using a Panalytical X'Pert Pro diffractometer. The Cu Kα radiation (wavelength, λ = 0.154 nm) was generated at 45 kV and 40 mA. All samples were scanned at a rate of 3°/min between 10° and 40° in reflectance mode. The crystallinity was determined by assuming that the total diffraction within a certain region of reciprocal space is independent of the state of aggregation of the material. The crystallinity, X_c, expressed as the mass fraction of the crystalline component, is then given as

$$X_c = \frac{A_c}{A_c + A_a} \quad (3)$$

where A_a is the area under the peaks corresponding to the amorphous region and A_c is the area remaining under the crystalline peaks.[21]

Thermodynamic and Mechanical Properties. The thermal behavior of the composite was measured using DSC (Seiko Instruments, Inc., DSC6100). The instrument was calibrated using known standards: indium (T_m = 165.8 °C) and zinc (T_m = 419.5 °C). The sample (2−3 mg) was packed into aluminum DSC sample pans with the lid tightly crimped. Measurements were taken between −50 and 200 °C at a scanning rate of 10 °C/min under a nitrogen gas flow.

The dynamic viscoelastic properties of the composite were measured in a tensile mode, using a dynamic viscoelastic analyzer (DVA-220, IT Keisoku Seigyo Co., Japan) with a chuck distance of 10 mm and a frequency of 10 Hz. The storage modulus (E'), loss modulus (E''), and loss tangent (tan δ) were measured as a function of temperature, using a heating rate of 5 °C/min.

The tensile tests were carried out using a screw-driven model Intesco Co. tensile machine (IM-20ST). The grip interval was 10 mm. All samples were deformed at 20 °C at a strain rate of 100%/min.

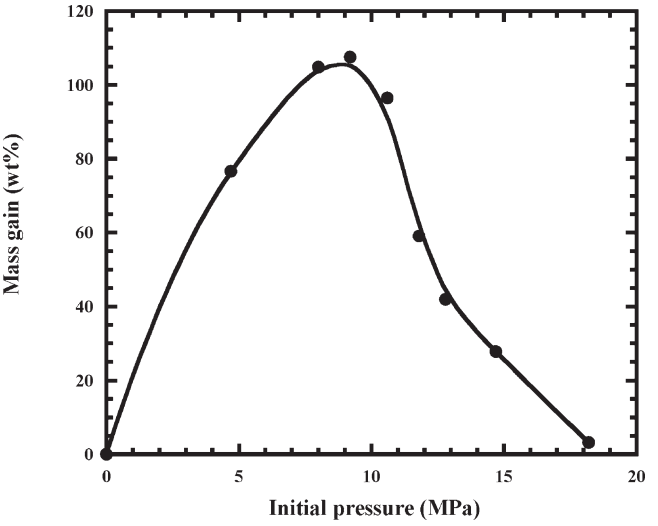

Figure 1. Effect of initial pressure on the mass gain of PMMA into PP substrate after polymerization.

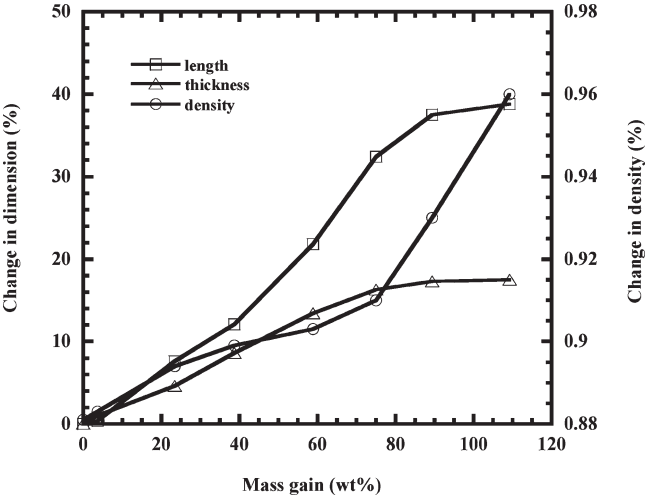

Figure 2. Changes in length, thickness, and density of PP/PMMA composites as a function of the mass gain of PMMA.

RESULTS AND DISCUSSION

Preparation of PP/PMMA Composite in $scCO_2$. Figure 1 shows the effect of the initial pressure of CO_2 on the mass gain of PMMA into the PP substrate after polymerization. The mass gain initially increases in correlation with the initial pressure, reaching a maximum of 109 wt % when the initial pressure of CO_2 is about 9 MPa, and then decreases with further increases in the initial pressure. Therefore, the mass gain of the PMMA sample can be controlled by modulating the initial pressure of CO_2. These results are similar to those obtained in our previous study.[5]

$ScCO_2$ is a good swelling agent and generally a poor solvent for most polymers. Impregnation of $scCO_2$ starts on the surface of the substrate followed by gradual permeation of the inner substrate. The swelling kinetics of CO_2 into the polymer matrix depends on both the temperature and pressure.[22,23] Differing from other polymers, PMMA possesses the swelling properties in CO_2 that depend on the temperature and pressure.[24] When the initial pressure of CO_2 is low, both the solubility of MMA and the

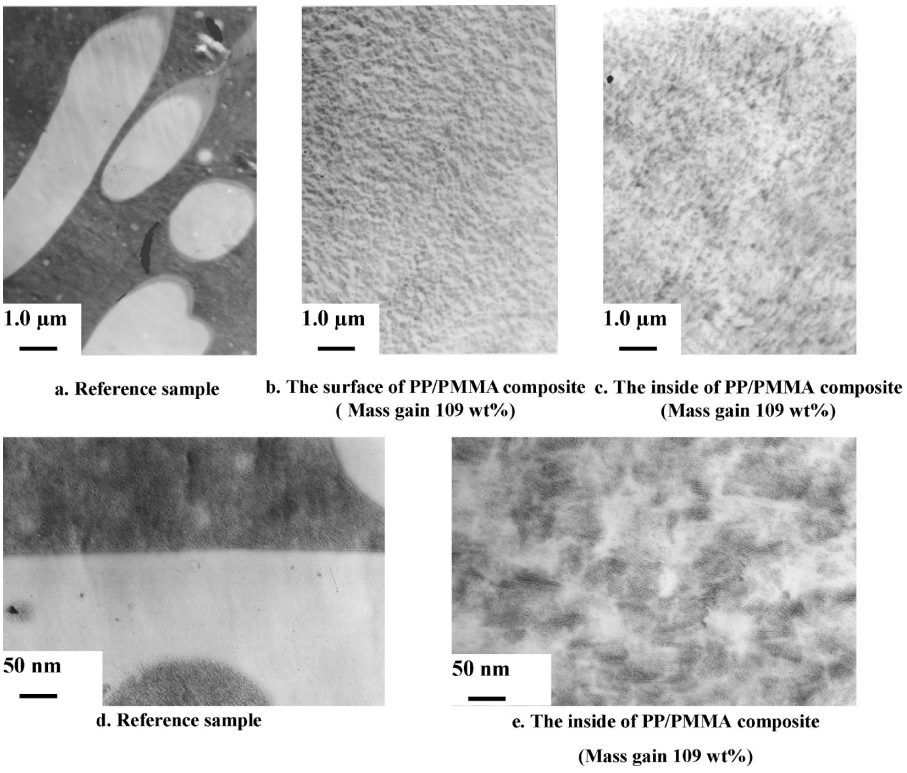

Figure 3. TEM images of reference sample and PP/PMMA composite (mass gain: 109 wt %).

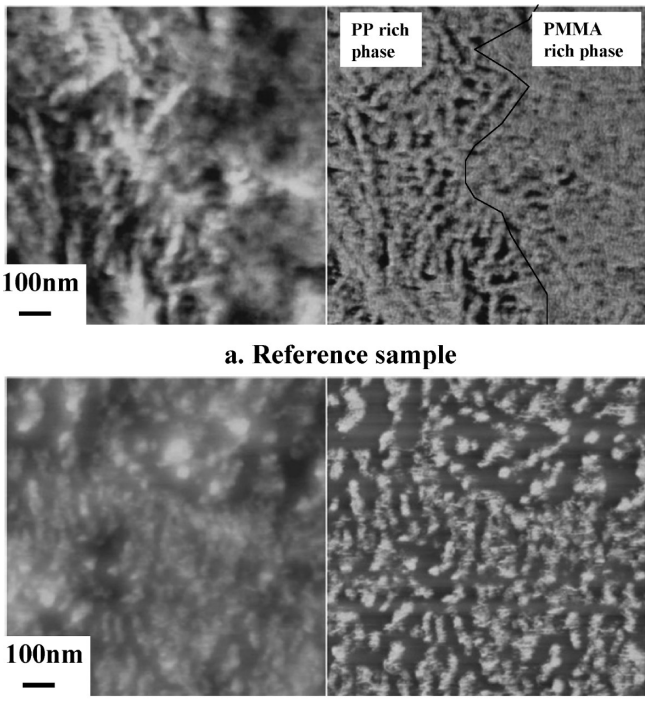

Figure 4. AFM height (left) and phase (right) images of reference sample and PP/PMMA composite (mass gain: 109 wt %).

swelling of the amorphous PP region are low, resulting in insufficient generation of PMMA in the PP substrate. An increase

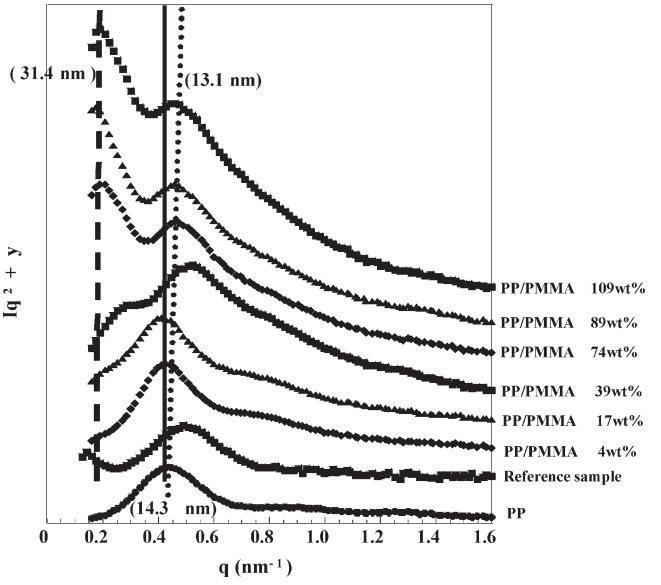

Figure 5. Plots of Lorenz-corrected SAXS intensity Iq^2 vs q of reference sample and PP/PMMA composites.

in the initial pressure results in improved solubility of MMA and swelling of the amorphous PP region, which results in an increase in the mass gain with higher initial pressures. However, the partition coefficient of MMA in CO_2 becomes larger than that in PP substrate at even higher pressures. Additionally, at high pressure, the rate of the decomposition of AIBN is relatively slow.[25,26] A combination of these factors explains the mass gain decreases with increasing initial pressures over 9 MPa.

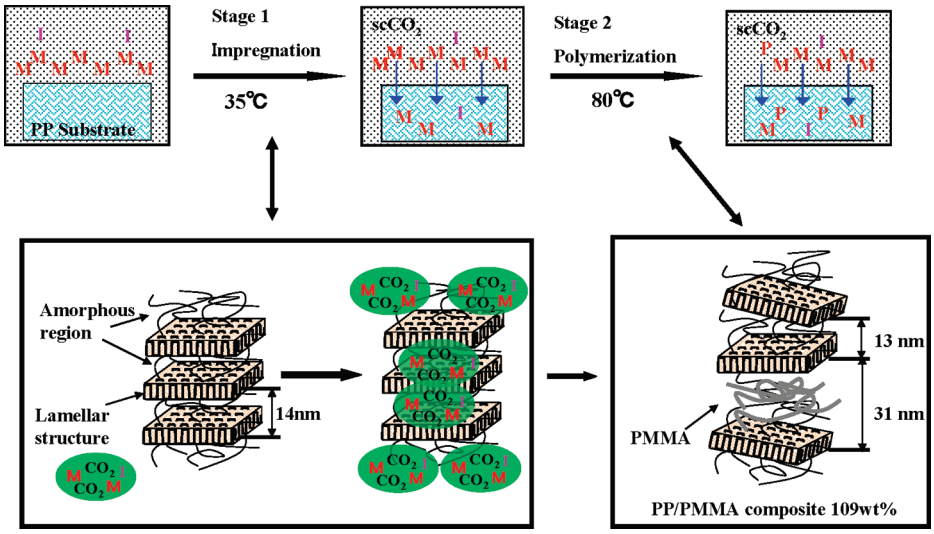

Figure 6. Formation mechanism model of PP/PMMA composite (M: monomer (MMA); P: polymer (PMMA); I: initiator (AIBN)).

We also note that after incorporation of PMMA the dimensions (length, thickness) of the specimens were found to have grown significantly from their initial substrate dimensions while retaining their original square shape (the lengths of four sides are almost same even after the polymerization). Figure 2 shows the changes in length, thickness, and density of the PP/PMMA composites as a function of the mass gain of PMMA. As expected, the higher the PMMA incorporation, the larger the final dimensions. Interestingly, although the dimensions show a nearly linear growth up until 75 wt %, the growth significantly slows after 75 wt %. PP and PMMA have densities of 0.881 and 1.19 g/cm^3, respectively, and the PP/PMMA composites with a mass gain of 75 and 109 wt % have densities of 0.910 and 0.960 g/cm^3, respectively. This demonstrates a significant increase in the density of the composites above 75 wt %, which is due to the constriction of the dimensions with increasing mass gain at this point. In addition, the interactions between the chains of generated PMMA occur gradually, after which the density of the PP/PMMA composite is closer to the density of PMMA.

GPC measurements indicate the molecular weight of PMMA produced inside of PP substrate is higher than that produced outside of PP substrate. PMMA from a 75 wt % PP/PMMA composite exhibited a $M_w = 62.3 \times 10^4$ with a PDI (M_w/M_n) = 1.9. The corresponding PMMA produced outside of PP substrate exhibited a $M_w = 5.8 \times 10^4$ with a PDI = 2.5. PMMA from a 109 wt % PP/PMMA composite exhibited a $M_w = 84.8 \times 10^4$ with a PDI = 1.6. The corresponding PMMA produced outside of PP substrate exhibited a $M_w = 6.5 \times 10^4$ with a PDI = 2.7. These results are similar to those obtained in the literature.[8]

Microstructure Analyses of the PP/PMMA Composite. Figure 3 displays TEM micrographs of the reference sample (PP/PMMA = 100/100) and PP/PMMA composite (mass gain: 109 wt %; PP/PMMA = 100/109). The dark portions in the micrographs are PP domains, and the light portions are PMMA domains. In the reference sample (a and d), large PMMA domains of micrometer scale were formed in the PP substrate and the phase boundary was clear. Conversely, in the PP/PMMA composite prepared by scCO$_2$ (b, c, and e), the PMMA domains are finely dispersed within the PP substrate on a nanometer scale and the phase boundary was ambiguous. Nevertheless, when the micrographs of both the reference sample and PP/PMMA composite are magnified (d and e), numerous streaks are evident. These streaks signify lamellar crystal of PP. This indicates that some portions of the original crystalline phases of PP are preserved throughout the preparation process.

Figure 4 shows the AFM height and phase images of the reference sample and the PP/PMMA composite (mass gain: 109 wt %). From the height images, it can be seen that the surface of the reference sample is rougher than that of the PP/PMMA composite. This may indicate that the scCO$_2$ impregnation assists in producing a more homogeneous internal structure of the polymer. The height image of the PP/PMMA composite also differs from that of the reference sample due to the presence of a granular-shaped feature. This change in topography is likely due to the incorporation of PMMA into PP, which results in a change in the internal structure of the PP. In the phase images, a strong contrast of bright and dark regions was observed for all samples. This is consistent with the fact that PP and the composite are semicrystalline polymers consisting of crystalline and amorphous phases with different moduli. The bright portions are attributed to the stiffer materials whereas the dark portions are attributed to the softer materials.[27,28] In the reference sample, the left side shows a strong contrast of bright and dark regions, which is attributed to the crystalline and amorphous phases of PP. Conversely, the right side shows only bright regions, which are attributed to PMMA. The phase boundary is clear. In contrast, in the PP/PMMA composite, the phase boundary is ambiguous and the amorphous regions of PP expand, as a result of the polymerization of PMMA within the amorphous regions.

Assuming that the morphology is globally isotropic but locally lamellar, the microstructural periodicity of the PP/PMMA composite and reference sample can be obtained from unoriented SAXS patterns. Figure 5 plots the scattering data in the form of the Lorenz-corrected SAXS intensity, Iq^2, versus the scattering vector, q, where I is the scattering intensity and q is defined by

$$q = \frac{4\pi}{\lambda} \sin \frac{\theta}{2} \tag{4}$$

where λ is the wavelength of the X-ray and θ is the scattering angle. The PP sample shows both first- and second-order

dx.doi.org/10.1021/ma2001965 |*Macromolecules* 2011, 44, 6103–6112

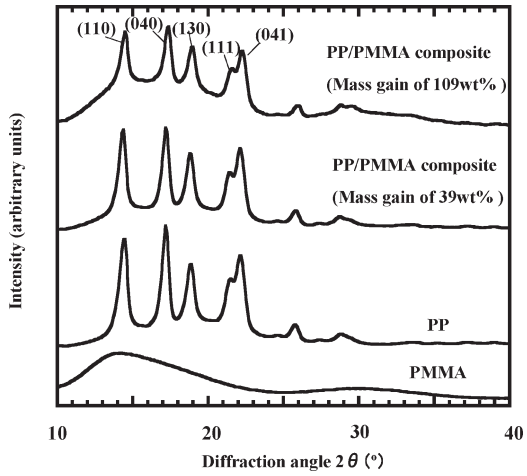

Figure 7. WAXD patterns of PMMA, PP, and PP/PMMA composites.

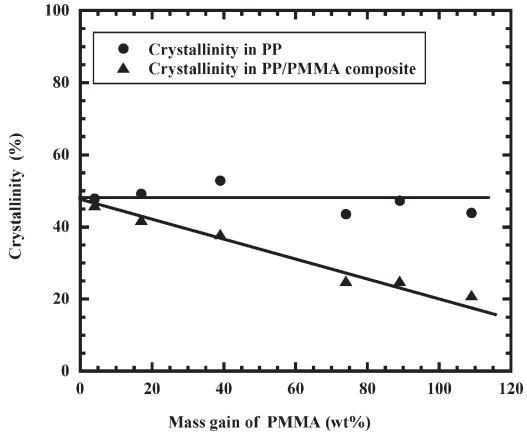

Figure 8. Relationship between crystallinity and mass gain of PMMA.

reflections, which are assigned to the long period corresponding to the sum of thickness of a crystalline layer, PPc, and an amorphous layer, PPa, in semicrystalline lamellae. This shows that the interface between the crystalline and amorphous regions is sharp, so the application of a two-phase model is appropriate. The Bragg spacing was estimated from the maximum q^* using the relation $d_1 = 2\pi/q^*$. The magnitude, d_1, of 14.3 nm for PP, estimated from $q^* = 0.439\ \mathrm{nm}^{-1}$, is comparable with the reported value of 15.3 nm.[29]

First- and second-order reflections are also observed in the reference sample. In this case, the scattering intensity for a q smaller than $0.3\ \mathrm{nm}^{-1}$ tends to increase as q decreases, which indicates the presence of large domains in the reference sample. These results are reasonable since the phases of PP and PMMA in the reference sample are macroscopically separated, as is shown in Figure 3a, and so the microstructure of PP would remain intact.

In the PP/PMMA composite, the SAXS profiles gradually change with increases in the mass gain of PMMA: The first-order reflection (approximately $q = 0.4\ \mathrm{nm}^{-1}$) tends to shift to a larger q and both intensities of the first- and second-order (approximately $q = 0.8\ \mathrm{nm}^{-1}$) reflection tend to become weaker, and the second-order reflection even disappears finally. (This can be seen clearly in Figure 11.) In the PP/PMMA composite with a

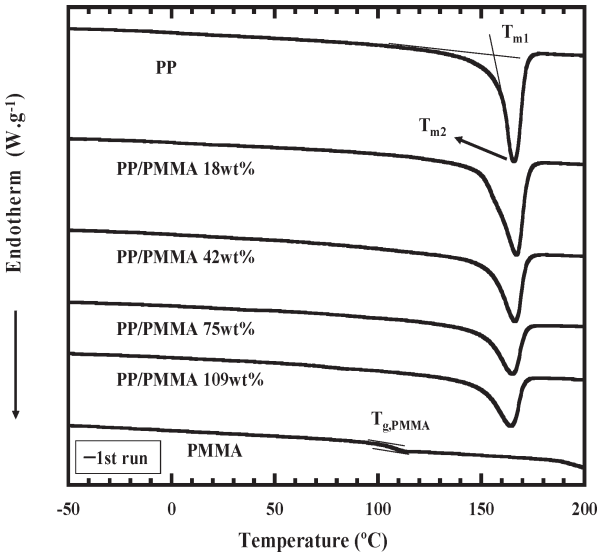

Figure 9. DSC thermograms of PP, PMMA, and PP/PMMA composites.

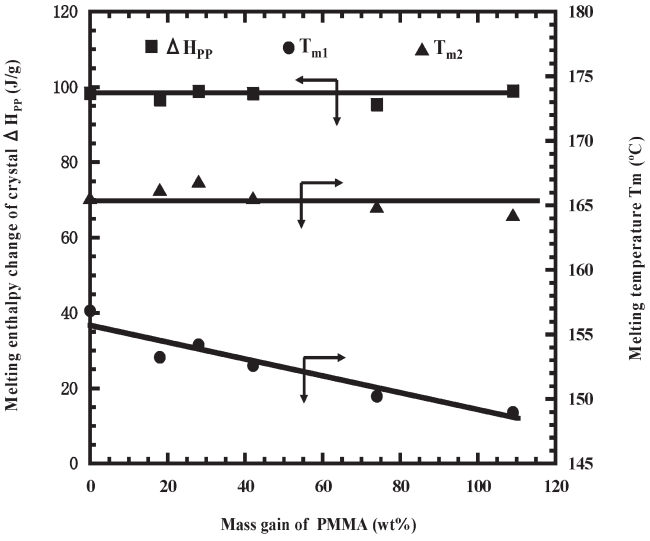

Figure 10. Relationship between the changes of melting enthalpy of PP crystal (ΔH_{PP}), melting temperature of PP/PMMA composite (T_m), and mass gain of PMMA.

mass gain of 17 wt %, a shoulder appears in a q range around $0.3\ \mathrm{nm}^{-1}$, which becomes a bump as the mass gain of PMMA increases up to a maximum of q of $\sim 0.20\ \mathrm{nm}^{-1}$ at 109 wt % mass gain, which corresponds to a dimension of ~31 nm. From these results, it is evident that MMA and AIBN, dissolved in $scCO_2$, are impregnated into the amorphous phase of PP and subsequently polymerized *in situ* to form new phases consisting of polymerized PMMA embedded in amorphous phases of PP. The structures of the rest of the amorphous phases and crystalline phases of PP are unchanged or only slightly modified, as shown in Figure 6.

On the basis of the results of TEM, AFM, and SAXS analyses, the mechanism of the formation of the PP/PMMA composite was established (Figure 6). In stage 1, the monomer and initiator were dissolved in $scCO_2$ and impregnated into the amorphous interlamellar regions of PP substrate. In stage 2, after reaching the polymerization temperature, the monomer polymerized within

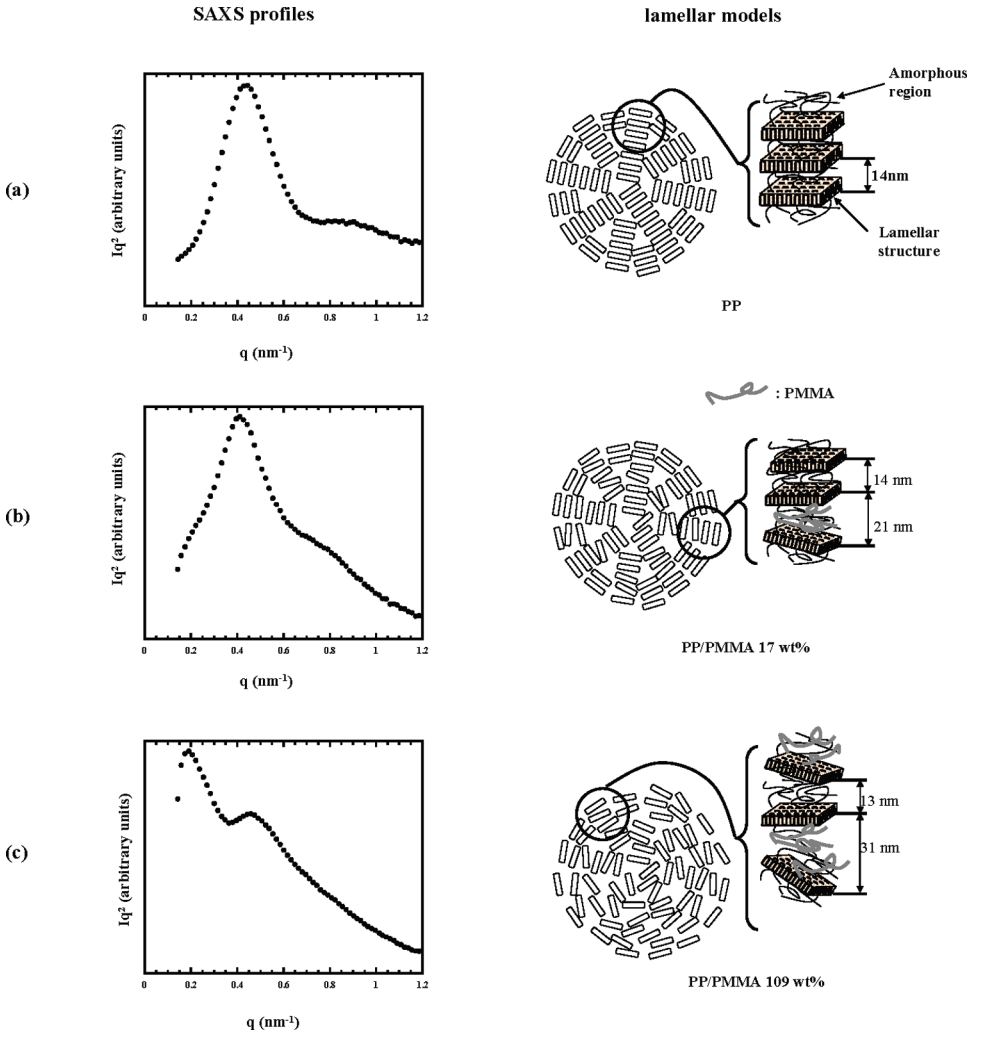

Figure 11. Corresponding relationship between SAXS profiles and lamellar models: (a) PP; (b) PP/PMMA composite 17 wt %; (c) PP/PMMA composite 109 wt %.

the amorphous interlamellar regions of PP substrate. The polymerization of monomer led to the imbalance of the partition coefficient of monomer within and outside of the PP substrate. The monomer outside of the PP substrate thus permeated into the amorphous regions of the PP substrate, and the polymerization reaction was continuous. As a result, PP and PMMA were effectively blended at the nanometer level.

Crystallinity of the PP/PMMA Composite. Figure 7 shows the WAXD patterns of PMMA, PP, and PP/PMMA composites. It can be seen that the WAXD patterns of both the PP and PP/PMMA composite present the characteristic peaks for the (110), (040), (130), (111), and (041) planes of the well-known α-form (monoclinic phase).[17,19,30,31] The angular positions of the diffraction peaks of the crystalline PP are almost identical for original PP substrate and for the PP/PMMA composite, indicating that the crystal forms are not changed upon the addition of PMMA. However, the amorphous regions of the PP/PMMA composite increased with the mass gain of PMMA, which indicates that the overall crystallinity decreases with increases in the mass gain of PMMA (Figure 8). The reduction in sample crystallinity is due to dilution as a result of the addition of PMMA to the amorphous PP regions and the resultant increase in the size of the amorphous regions. Percent crystallinity in PP, X_{PP}, was calculated as follows:

$$X_{PP}\ (\%) = \frac{X_{PP/PMMA}}{W_{PP}} \qquad (5)$$

where X_{PP} is the crystallinity of PP/PMMA composite assumed to be dependent only on the crystalline regions of PP, $X_{PP/PMMA}$ is the crystallinity of the PP/PMMA composite, and W_{PP} is the weight fraction of PP. X_{PP} does not change, although $X_{PP/PMMA}$ decreases according to an increase in the mass gain of PMMA. The total amount of crystalline PP remains unchanged. These results indicate that the MMA polymerizes solely within the amorphous regions of the polymer.

Thermodynamic and Mechanical Properties of the PP/PMMA Composite. Differential scanning calorimetry, shown in Figure 9, confirmed the WAXD data. In PP/PMMA composites, strong PP melting endotherms were observed. The melting endotherms reveal that the composite preparation does not affect the crystalline region of the PP substrate. Further, the melting endotherm peaks became broad and shallow with increasing mass gain of PMMA. This is due entirely to dilution of the crystalline regions by the addition of PMMA to amorphous PP regions. Although the top temperature of the melting

dx.doi.org/10.1021/ma2001965 |*Macromolecules* 2011, 44, 6103–6112

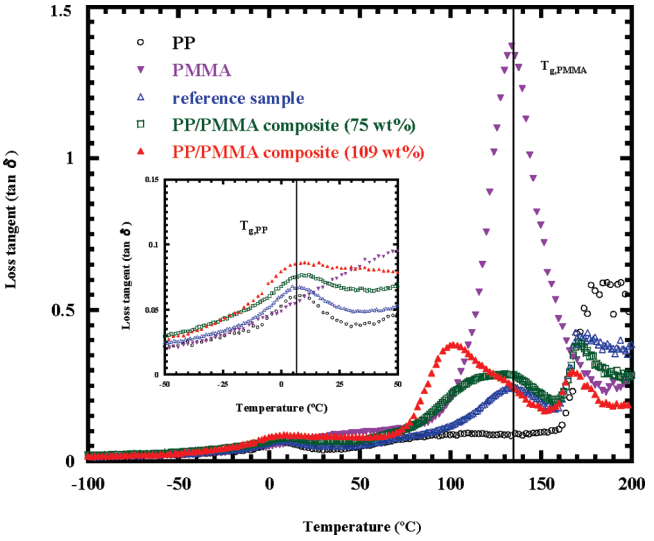

Figure 12. Temperature dispersion curves of the loss tangent (tan δ) for original PP, PMMA, reference sample, and PP/PMMA composites.

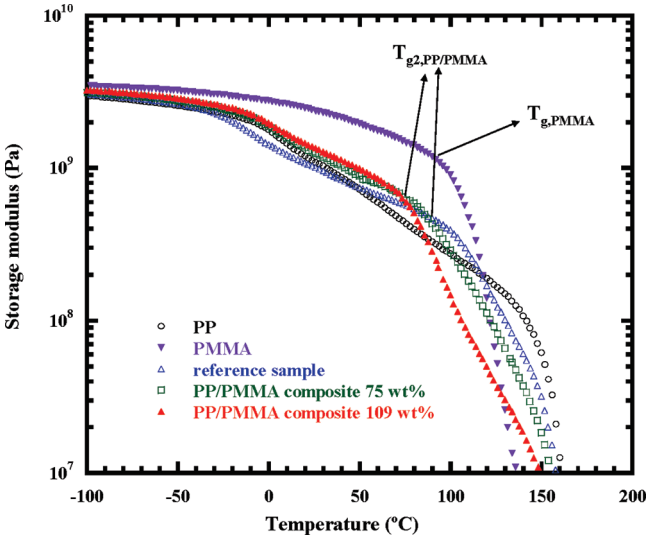

Figure 14. Temperature dispersion curves of the storage modulus (E') for original PP, PMMA, reference sample, and PP/PMMA composites.

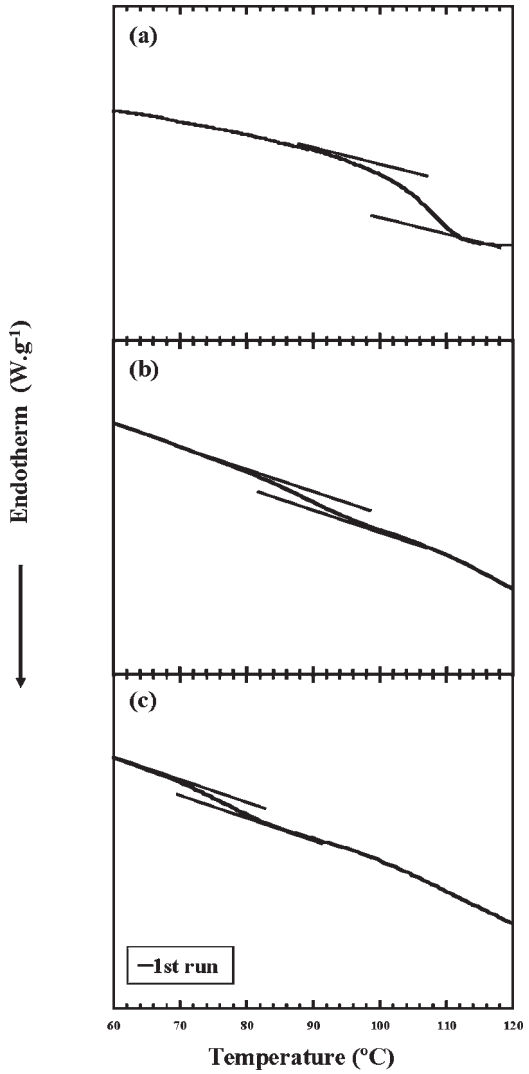

Figure 13. Enlargement of DSC thermograms of PMMA and PP/PMMA composites: (a) PMMA; (b) PP/PMMA 75 wt %; (c) PP/PMMA 109 wt %.

endotherm peaks (T_{m2}) was not significantly affected by the mass gain of PMMA, the starting temperature of melting endotherm peaks (T_{m1}) decreased with the mass gain of PMMA, as shown in Figure 10. Generally, a decrease in T_{m1} is caused by changes in the kinds of crystals or crystallinity of the sample. However, the WAXD data confirmed that the crystal types and crystallinity are independent of the addition of PMMA (Figures 7 and 8). It is possible that the decrease in T_{m1} can be explained by the formation mechanism of the PP/PMMA composite, as was discussed in microstructure analyses. From the SAXS profiles, slight changes in the lamellar structure can be postulated. Figure 11 shows the corresponding relationship between the SAXS profiles and lamellar models. In PP, both the first- and second-order reflections are evident. In the PP/PMMA composite with a mass gain of 17 wt %, a shoulder appears at a q of ~0.3 nm^{-1}, which corresponds to a relatively large dimension of ~21 nm. Because the mass of PMMA is relatively low, most of the PP lamellar structures are retained, and the first- and second-order reflections can still be observed, although they are weak. However, in the PP/PMMA composite with a mass gain of 109 wt %, a strong peak appears at a q of ~0.2 nm^{-1}, which corresponds to a larger dimension of ~31 nm, and the first-order reflection is weaker, while the second-order reflection is not observed. As the amount of crystal is constant, the formation of new lamellar structures causes the reflections originating from the PP lamellar to weaken or even disappear. The changes of T_{m1} and T_{m2} are attributed to changes in the microstructure; as the volume of the amorphous regions of PP increase, melting the crystal is more facile, so T_{m1} decreases with the mass gain of PMMA. However, because the amorphous regions of PP were slightly modified by PMMA, T_{m2} did not change significantly with the mass gain of PMMA. Accordingly, the enthalpy change of the melting of the PP crystal, ΔH_{PP}, was calculated as follows:

$$\Delta H_{PP} = \frac{\Delta H_{PP/PMMA}}{W_{PP}} \quad (6)$$

where $\Delta H_{PP/PMMA}$ is the enthalpy change of the melting of the PP/PMMA composite crystal, which was assumed to be dependent only on the crystalline regions of PP. The relationship

dx.doi.org/10.1021/ma2001965 |*Macromolecules* 2011, 44, 6103–6112

Table 1. Results of Tensile Tests

sample name	yield stress (MPa)	fracture stress (MPa)	fracture strain (%)
PP	31	30	1290
PP/PMMA composite (17 wt %)	34	36	1000
PP/PMMA composite (28 wt %)	37	35	860
PP/PMMA composite (59 wt %)	38	33	90
PP/PMMA composite (74 wt %)	38	33	55
PP/PMMA composite (109 wt %)	38	34	30
reference sample		27	4
PMMA		42	5

between ΔH_{PP} and the mass gain of PMMA is shown in Figure 10. It is evident that ΔH_{PP} is constant with the mass gain of PMMA. This is further confirmation that the total amount of PP crystal does not change upon the addition of PMMA, which is in accord with the results of WAXD. These results indicate that although the addition of PMMA does not affect the enthalpy change of the melting of the PP crystal or the top temperature of PP crystal melting, it did reduce the temperature at which the PP crystal begins to melt.

The measurement of dynamic viscoelastic behavior is an effective method of evaluating the miscibility of two components through the determination of the glass transition temperature, T_g, of the respective components. Figure 12 shows the temperature dispersion curves of the loss tangent (tan δ) for PP, PMMA, the reference sample, and the PP/PMMA composites. For PP, the α-relaxation peak appeared at ∼0 °C corresponding to the T_g of the PP amorphous chain ($T_{g,PP}$). For PMMA, the α-relaxation peak appeared at ∼130 °C, which corresponds to the T_g of the PMMA chain ($T_{g,PMMA}$). Because PP and PMMA are immiscible, the peaks in the reference sample correspond to those of PP and PMMA. The analysis of the PP/PMMA composite also showed the three peaks which correspond to $T_{g,PP}$, $T_{g,PMMA}$ and T_m of PP ($T_{m,PP}$). The two peaks corresponding to $T_{g,PP}$ and $T_{g,PMMA}$ are shifted with respect to each other: The $T_{g,PP}$ peak ($T_{g1,PP/PMMA}$) was shifted toward a higher temperature, while the $T_{g,PMMA}$ peak ($T_{g2,PP/PMMA}$) shifted toward a lower temperature. Further, the shifting extent increased with increasing the mass gain of PMMA. This is also observed in DSC thermograms (Figure 13). Although it is hard to see the $T_{g,PP}$ by DSC, the $T_{g,PMMA}$ component can be observed in the enlargement of DSC. With increasing the mass gain of PMMA, the $T_{g,PMMA}$ was shifted toward a lower temperature. These results imply that, using this method, the PP and PMMA polymers were somewhat thermodynamically miscible.[32]

Figure 14 shows the temperature dispersion curves of the storage modulus (E') of PP, PMMA, the reference sample, and the PP/PMMA composites. At temperatures lower than $T_{g2,PP/PMMA}$, the E' of the PP/PMMA composite was larger than that of PP. Conversely, at temperatures higher than $T_{g,PMMA}$, the E' of the PP/PMMA composite was smaller than that of PP. Therefore, the change of E' occurs between the $T_{g2,PP/PMMA}$ and $T_{g,PMMA}$. The temperature dependence of E' can be explained via the mobility of the polymer chain. At temperatures lower than $T_{g2,PP/PMMA}$, the chain mobility of the amorphous regions of PP was prevented by the glassy PMMA generated in the amorphous regions. The E' of PMMA was larger than that of PP at temperatures lower than $T_{g2,PP/PMMA}$. Therefore, the lowered mobility of the amorphous PP chains resulted in the E' of the PP/PMMA composite being higher than that of PP. At temperatures higher than $T_{g,PMMA}$, the amorphous regions of PP/PMMA composite increased to more than that of PP to allow micro-Brownian motion of the PMMA. Therefore, the E' of PMMA decreased quickly so that the E' of the PP/PMMA composite was smaller than that of PP. Similarly, the changes of E' of PP/PMMA composites can be also explained via the mobility of the polymer chain. Namely, the E' of PP/PMMA composite can be controlled through the mass gain of PMMA.

Table 1 lists the results of the tensile test at 20 °C. In the reference sample, a macrophase separation was induced because PP and PMMA are immiscible. The conversion of the sample to a macrophase-separated structure was usually had a deleterious effect on its mechanical properties. However, the yield stress of the PP/PMMA composites is considerably higher than that of PP. Further, it increased gradually with the mass gain of PMMA and reached a plateau at a mass gain of 59 wt %. The fracture stress of the PP/PMMA composites is also improved as compared to that of PP. In addition, the fracture strain decreased rapidly with the mass gain of PMMA. Therefore, nanometer-sized PMMA generated in the amorphous regions significantly affected the mechanical properties of PP/PMMA composite, which can be controlled through the mass gain of PMMA.

CONCLUSION

We prepared a new composite composed of PP and PMMA by *in situ* polymerization of MMA using $scCO_2$. PMMA was generated in the amorphous regions between the crystalline lamellae of PP. PMMA generated in the amorphous region of PP did not affect its crystallinity, the enthalpy of melting the PP crystal, or the top temperature of PP crystal melting, but it did reduce the starting temperature of PP crystal melting. Experimental evidence demonstrates that the PP and PMMA were blended at the nanometer level and achieved thermodynamic miscibility to some extent. PMMA generated in the amorphous regions of PP substrate significantly affected the viscoelastic and mechanical properties of the PP/PMMA composite. At temperatures lower than $T_{g2,PP/PMMA}$, the E' of the PP/PMMA composite was larger than that of PP. At temperatures higher than $T_{g,PMMA}$, the E' of the PP/PMMA composite was smaller than that of PP. Mechanical properties such as yield stress, fracture stress, and strain can be controlled by changing the mass gain of PMMA. Thus, new materials with enhanced mechanical properties can be developed by tuning the conditions such as the ratio of the blending polymer and the type of polyolefin and blending polymer.

REFERENCES

(1) Han, C. C.; Bauer, B. J.; Clark, J. C.; Muroga, Y.; Matsushita, Y.; Okada, M.; Tran-cong, Q.; Chang, T. *Polymer* **1988**, *29*, 2002–2014.

(2) *Polymer Blend*; Akiyama, S., Inoue, T., Nishi, T., Eds.; CMC Publishing: Tokyo, 1981; p 56.
(3) Watkins, J. J.; McCarthy, T. J. *Macromolecules* **1994**, *27*, 4845–4847.
(4) Hoshi, T.; Sawaguchi, T.; Konno, T.; Takai, M.; Ishihara, K. *Polymer* **2007**, *48*, 1573–1580.
(5) Sawaguchi, T.; Muroga, Y.; Ishikawa, H.; Hoshi, T.; Hagiwara, T.; Yano, S. *Kobunshi Ronbunshu* **2005**, *62*, 251–260.
(6) Li, D.; Liu, Z.; Han, B.; Song, L.; Yang, G.; Jiang, T. *Polymer* **2002**, *43*, 5363–5367.
(7) Watkins, J. J.; McCarthy, T. J. *Macromolecules* **1995**, *28*, 4067–4074.
(8) Kung, E.; Lesser, A. J.; McCarthy, T. J. *Macromolecules* **1998**, *31*, 4160–4169.
(9) Zhang, J.; Busby, A. J.; Roberts, C. J.; Chen, X.; Davies, M. C.; Tendler, S. J. B.; Howdle, S. M. *Macromolecules* **2002**, *35*, 8869–8877.
(10) Busby, A. J.; Zhang, J.; Naylor, A.; Roberts, C. J.; Davies, M. C.; Tendler, S. J. B.; Howdle, S. M. *J. Mater. Chem.* **2002**, *13*, 2838–2844.
(11) Naylor, A.; Howdle, S. M. *J. Mater. Chem.* **2005**, *13*, 2838–2844.
(12) Busby, A. J.; Zhang, J.; Roberts, C. J.; Lester, E.; Howdle, S. M. *Adv. Mater.* **2005**, *17*, 364–367.
(13) Naylor, A.; Timashev, P. S.; Solov'eva, A. B.; Erina, N. A.; Kotova, S.; Busby, A. J.; Popov, V. K.; Howdle, S. M. *Adv. Mater.* **2008**, *20*, 575–578.
(14) *Polymer Handbook*; Brandrup, J., Immergut, E. H., Grulke, E. A., Abe, A., Bloch, D. R., Eds.; Wiley-Interscience: New York, 1999; pp 159−161.
(15) ÓKane, W.; Young, R. J.; Ryan, A. J. *J. Macromol. Sci., Part B: Phys.* **1995**, *B34*, 427–458.
(16) Poussin, L.; Bertin, Y. A.; Parisot, J.; Brassy, C. *Polymer* **1998**, *39*, 4261–4265.
(17) Ferrer-Balas, D.; Maspoch, M. L.; Martinez, A. B.; Santana, O. O. *Polymer* **2001**, *42*, 1697–1705.
(18) Aboulfaraj, M.; ĠSell, C.; Ulrich, B.; Dahoun, A. *Polymer* **1995**, *36*, 731–742.
(19) Seguela, R.; Staniek, E.; Escaig, B.; Fillon, B. *J. App. Polym. Sci.* **1999**, *71*, 1873–1885.
(20) Muroga, Y.; Tagawa, H.; Hiragi, Y.; Ueki, T.; Kataoka, M.; Izumi, Y.; Amemiya, Y. *Macromolecules* **1988**, *21*, 2756–2760.
(21) Ryan, A. J.; Stanford, J. L.; Bras, W.; Nye, T. M. W. *Polymer* **1997**, *38*, 759–768.
(22) Nikitin, L. N.; Said-Galiyev, E. E.; Vinokur, R. A.; Khokholov, A. R.; Gallyamov, M. O.; Schaumburg, K. *Macromolecules* **2002**, *35*, 934–940.
(23) Royer, J. R.; DeSimone, J. M.; Khan, S. A. *Macromolecules* **1999**, *32*, 8965–8973.
(24) Sirard, S. M.; Ziegler, K. J.; Sanchez, I. C.; Green, P. F.; Johnston, K. P. *Macromolecules* **2002**, *35*, 1928–1935.
(25) Desimone, J. M.; Guan, Z.; Elsbernd, C. S. *Science* **1992**, *257*, 945–947.
(26) Guan, Z.; Combes, J. R.; Menceloglu, Y. Z.; DeSimone, J. M. *Macromolecules* **1993**, *26*, 2663–2669.
(27) Bar, G.; Thomann, Y.; Whangbo, M. H. *Langmuir* **1998**, *14*, 1219–1226.
(28) Sauer, B. B.; McLean, R. S.; Thomas, R. R. *Langmuir* **1998**, *14*, 3045–3051.
(29) Berens, A. R.; Huvard, G. S.; Korsmeyer, R. W.; Kunig, F. W. *J. Appl. Polym. Sci.* **1992**, *46*, 231–242.
(30) Natta, G.; Corradini, P. *Nuovo Cimento, Suppl.* **1960**, *15*, 40–51.
(31) Natta, G.; Peraldo, M.; Corradini, P. *Rand. Accad. Naz. Lincei* **1959**, *26*, 14–17.
(32) *Polymer Alloys and Blends*; Leszek, A. U., Ed.; Hanser: New York, 1989; p 4.